JACS
JOURNAL OF THE AMERICAN CHEMICAL SOCIETY

Article

pubs.acs.org/JACS

Transition-Metal Oxos as the Lewis Basic Component of Frustrated Lewis Pairs

Nikola S. Lambic, Roger D. Sommer, and Elon A. Ison*

Department of Chemistry, North Carolina State University, 2620 Yarbrough Drive, Raleigh, North Carolina 27695-8204, United States

Supporting Information

ABSTRACT: The reaction of oxorhenium complexes that incorporate diamidopyridine (DAP) ligands with $B(C_6F_5)_3$ results in the formation of classical Lewis acid−base adducts. The adducts effectively catalyze the hydrogenation of a variety of unactivated olefins at 100 °C. Control reactions with these complexes or $B(C_6F_5)_3$ alone did not yield any hydrogenated products under these conditions. Mechanistic studies suggest a frustrated Lewis pair is generated between the oxorhenium DAP complexes and $B(C_6F_5)_3$, which is effective at olefin hydrogenation. Thus, we demonstrate for the first time that the incorporation of a transition-metal oxo in a frustrated Lewis pair can have a synergistic effect and results in enhanced catalytic activity.

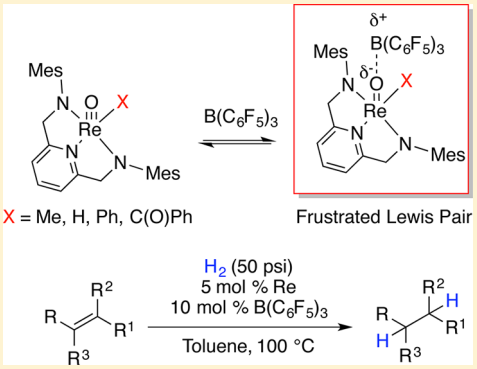

INTRODUCTION

In recent years the chemistry of frustrated Lewis pairs (FLPs) has emerged as a powerful new strategy for the development of catalysts for a variety of different reactions.[1] While most of the research effort has focused on the development of metal-free catalysts, there have been a few studies aimed at investigating the development of transition metals as the Lewis base or Lewis acid component of FLPs.[2]

We have recently shown that oxorhenium complexes that incorporate diamidoamine (DAAm) and diamidopyridine (DAP) ligands exhibit ambiphilic reactivity, in that, the metal oxo reacts with both Lewis acids and bases.[3] The reaction of these oxorhenium complexes with $B(C_6F_5)_3$ results in the formation of classical Lewis acid−base adducts. As shown in Figure 1, DFT(B3PW91)[4] calculated structures for $((C_6F_5)_3B(O)Re(DAP)(X))$ (DAP = (2,6- bis((mesitylamino)methyl)-pyridine) X = H, Me, Ph) reveal that as the size of the X-type ligand increases, steric interactions between the substituent on the diamidopyridine nitrogen, (mesityl) and the C_6F_5 groups of $B(C_6F_5)_3$ increases. Further, the formation of $((C_6F_5)_3B(O)Re(DAP)(Ph))$ is approximately 5 kcal/mol less endergonic than $((C_6F_5)_3B(O)Re(DAP)(H))$ and $((C_6F_5)_3B(O)Re(DAP)(Me))$. Thus, the weak association between the Lewis acid and the oxo ligands could result in complexes that exhibit the high latent reactivity that is common for traditional main group FLPs.[1f,5]

In this manuscript, we show that FLPs generated from (O)Re(DAP)(X) are efficient catalysts for the hydrogenation of unactivated olefins.[6] Thus, we demonstrate for the first time that the incorporation of a transition-metal oxo in a FLP results in enhanced catalytic activity, in contrast to when the transition-metal oxos, or $B(C_6F_5)_3$, by themselves were used as catalysts.

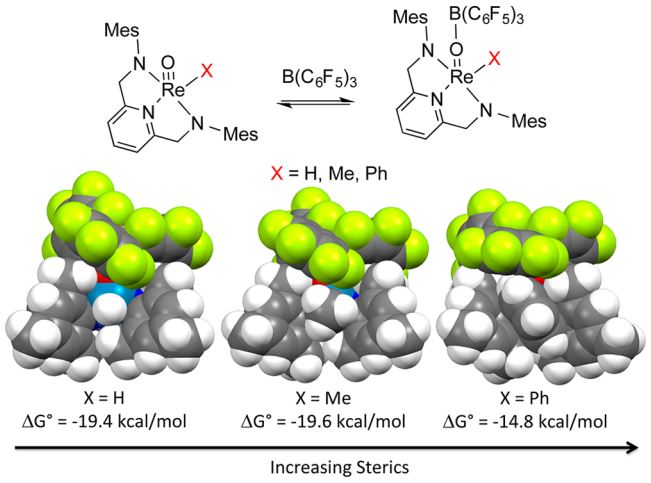

Figure 1. B3PW91[4] calculated structures for $((C_6F_5)_3B(O)Re(DAP)(X))$ (X = H, Me, Ph). Structures were optimized in the gas phase with the 6-31G* basis set[7] on C, H, N, O, F, and B and the SDD basis set and effective core potential on Re.[8] Energies also included Grimme's D3 dispersion corrections[9] as implemented in Gaussian 09[10] and solvent corrections by utilizing the PCM solvation model[11] with dichloromethane as the solvent.

RESULTS AND DISCUSSION

Synthesis of FLPs from Transition-Metal Oxos. *Synthesis of $((C_6F_5)_3B(O)Re(DAP)(Ph))$.* The stoichiometric reac-

Received: January 20, 2016
Published: March 22, 2016

DOI: 10.1021/jacs.6b00705
J. Am. Chem. Soc. 2016, 138, 4832−4842

tion of (O)Re(DAP)(Ph), **1**, with $B(C_6F_5)_3$ leads to the formation of the classical Lewis acid–base adduct, $((C_6F_5)_3)B$-(O)Re(DAP)(Ph)), **2**, (Scheme 1). Similar reactivity was

Scheme 1. Synthesis of 2

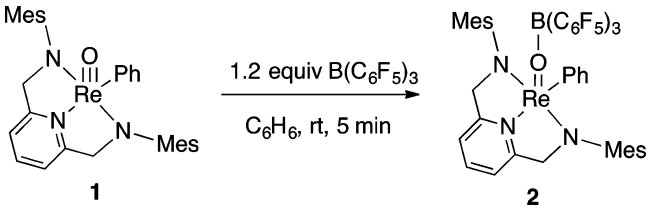

observed for other oxorhenium complexes published by our group.[3] This moisture-sensitive complex was isolated in 63% yield and exhibits the characteristic splitting pattern of the diastereotopic methylene protons syn (5.7 ppm) and anti (4.9 ppm) to the rhenium oxo, by ^{1}H NMR spectroscopy.

X-ray quality crystals of **2** were obtained by cooling a benzene/pentane solution of the complex to −40 °C (Figure 2). Rhenium

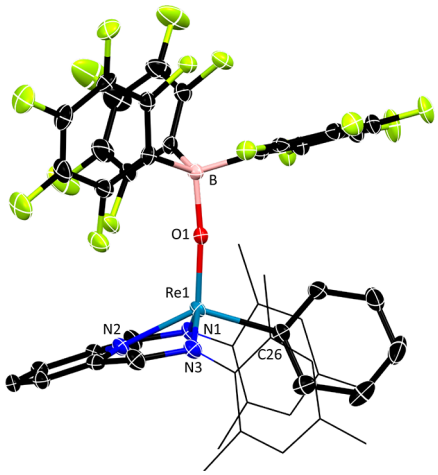

Figure 2. Thermal ellipsoid plot for **2**. Ellipsoids are at the 50% probability level. Hydrogen atoms were omitted for clarity, and the mesityl substituents are depicted in wireframe. Selected bond lengths (Å) and angles (deg). Re1–O1, 1.7674(17); Re1–N3, 1.963(2); Re1–N1, 1.954(2); Re1–N2, 2.050(2); O1–B, 1.535(3); Re1–C26, 2.084(3); Re1–O1–N1, 113.95(9); O1–Re1–N3, 111.25(8); N1–Re1–N3, 134.14(9); O1–Re1–N2, 118.28(8); N1–Re1–N2, 75.92(9); N3–Re1–N2, 76.47(9); O1–Re1–C26, 104.27(9); B–O1–Re1, 172.64(17).

occupies a distorted square pyramidal geometry in this molecule with the oxo ligand as well as $B(C_6F_5)_3$ in the apical position. As shown in Figure 2, the solid-state structure of **2** is sterically crowded, as the phenyl group is no longer parallel with the mesityl groups as seen in the structure for **1**. The angle of distortion is approximately 22.4°. The symmetry of the boron atom is also quite different than in other examples of acid–base adducts,[3] with one $-C_6F_5$ unit completely in the plane with the pyridine ligand and the other two perpendicular to the plane.

Dynamic Equilibrium with $B(C_6F_5)_4$. A variable-temperature ^{1}H and ^{19}F NMR analysis of a toluene-d_8 solution of a 1:1 mixture of **2**/$B(C_6F_5)_3$ provided evidence for a dynamic equilibrium in solution. For example, distinct signals for $B(C_6F_5)_3$ and **2** were observed in the ^{19}F NMR spectrum at room temperature (21 °C) at −132 (*ortho*-C_6F_5, **2**) and −129 (*ortho*-C_6F_5, borane) ppm, respectively. As the temperature was increased, these signals broadened and coalesced at ca. 51 °C. Cooling the solution to room temperature resulted in the original spectrum (see Figure S13). Similar dynamic behavior was observed by ^{1}H NMR spectroscopy. The data provide strong evidence for a dynamic equilibrium between **2** and $B(C_6F_5)_3$, as shown in Scheme 2. From the chemical shifts and the coalescence temperature the free energy of activation, ($\Delta G^{\ddagger}$ = 14.1 kcal/mol) can be estimated for this process.[12]

Scheme 2. Equilibrium between 2 and $B(C_6F_5)_3$

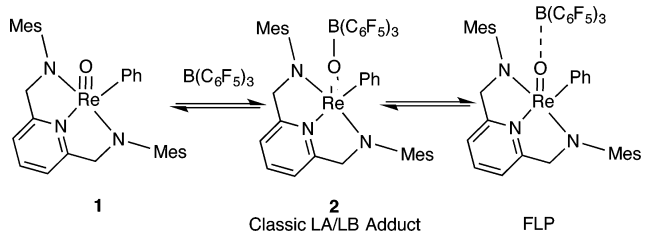

H/D Exchange. A toluene-d_8 solution of **2** was exposed to 60 psi (total pressure) of a 1:1 mixture of H_2/D_2 in a J-Young tube at 100 °C. ^{1}H NMR analysis of the mixture after 90 min showed signals consistent with the catalytic isotopic scrambling of hydrogen and deuterium (Figure 3). Equilibration was not observed when solutions of $B(C_6F_5)_3$ alone were employed.

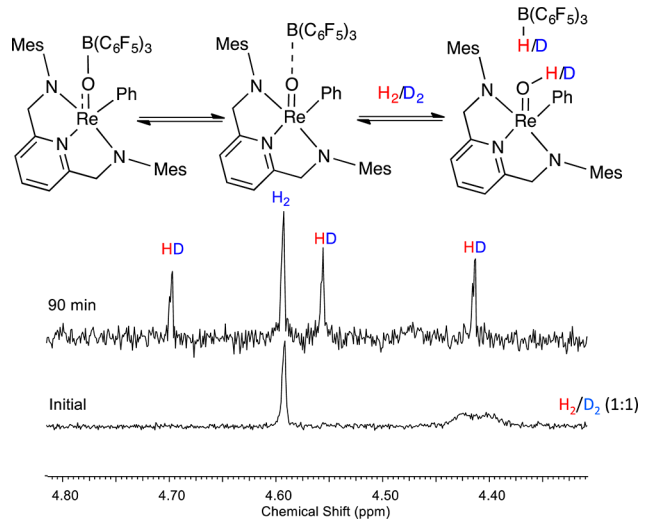

Figure 3. ^{1}H NMR spectra showing (A) the initial spectrum for a 1:1 mixture of H_2 and D_2 in the presence of **2** and 1 equiv of $B(C_6F_5)_3$ and (B) complete isotope scrambling of the H_2/D_2 mixture by 1:1 **2**/$B(C_6F_5)_3$ after 90 min in toluene-d_8.

To summarize, complex **1** forms the classic Lewis acid–base adduct **2** with $B(C_6F_5)_3$. Upon thermal activation, a FLP is generated that is capable of activating H_2. This reactivity is consistent with previously reported FLP reactivity.[1m,o,q,r]

Catalytic Hydrogenation with Transition-Metal Oxos. *Substrate Scope.* The combination of **1** and $B(C_6F_5)_3$ effectively catalyzes the hydrogenation of a variety of terminal, internal, cyclic, and conjugated olefins at 100 °C under the optimized conditions (Chart 1). Neither complex **1** nor $B(C_6F_5)_3$ catalyzes the hydrogenation of olefins under the optimized reaction conditions. Hydrogenation occurred smoothly for many of the small-linear-sterically unhindered alkenes, such as ethylene, and

DOI: 10.1021/jacs.6b00705
J. Am. Chem. Soc. 2016, 138, 4832–4842

Chart 1. Substrate Scope for Hydrogenation with 1/$B(C_6F_5)_3$[a]

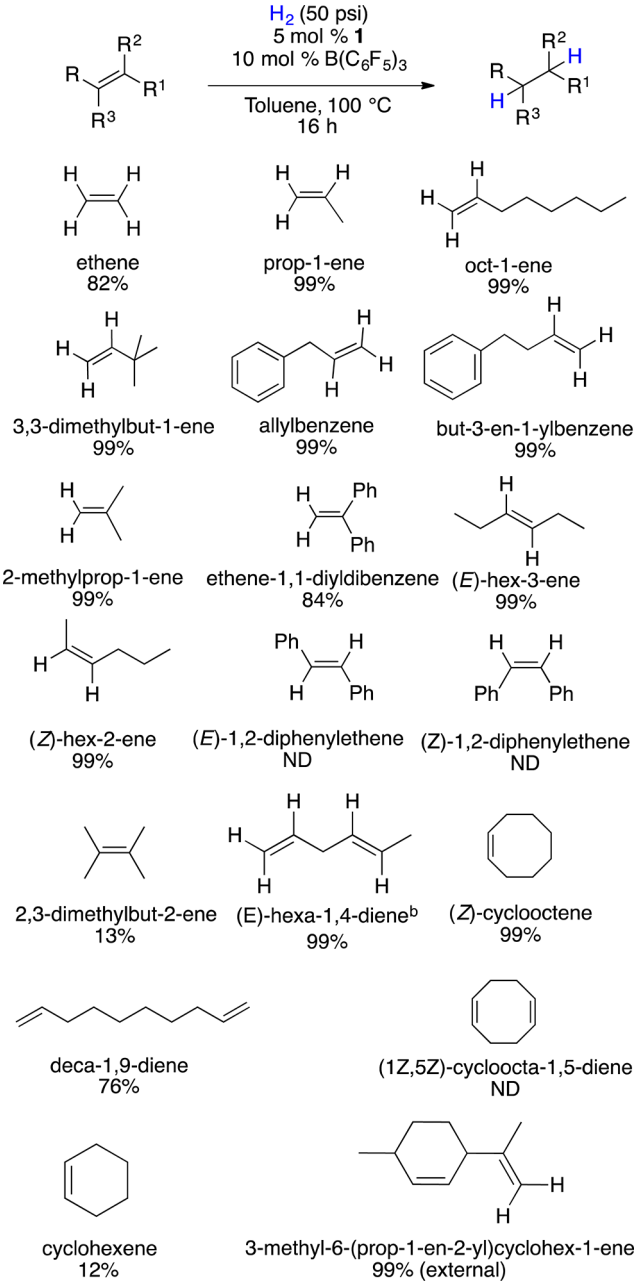

[a](a) %Conversion determined by integrating alkenic protons with respect to the corresponding methylene or methyl protons of the product. Conditions: **1** (0.0061 mmol), $B(C_6F_5)_3$ (0.0124 mmol), olefin (0.1224 mmol), toluene (0.2 mL) in a 3 mL storage tube. (b) Reaction resulted in a mixture of hexane (33%) and 3-hexene and 2-hexene (66%).

monosubstituted olefins, such as propylene, 1-octene, 3,3-dimethylbut-1-ene, allylbenzene, and 4-phenyl-1-butene. In all cases, high conversion was achieved in 16 h.

The use of geminal substituted olefins such as isobutylene (99%) and 1,1-diphenylethylene (84%) resulted in good conversion as well. The use of the vicinal substituted olefins, (*E*)-3-hexene (99%) and (*Z*)-2-hexene (99%), also proceeded efficiently. However, no alkane was detected when *cis*- and *trans*-stilbene were utilized. The tetrasubstituted olefin tetramethylethylene was utilized, however low yields (13%) were observed. The hydrogenation of the cyclic olefin cyclooctene was achieved with 99% conversion. However, low conversions (12%) were observed for cyclohexene, and cyclooctadiene was not hydrogenated. Dienes, 1−4 hexadiene (99%)[13] and 1−9 decadiene (76%) were also successfully hydrogenated.

Kinetic and Mechanistic Studies. Kinetic studies were performed using **1**/$B(C_6F_5)_3$ under optimized conditions (Scheme 3). Rate data were collected in order to determine

Scheme 3. Conditions for Hydrogenation of Neohexene

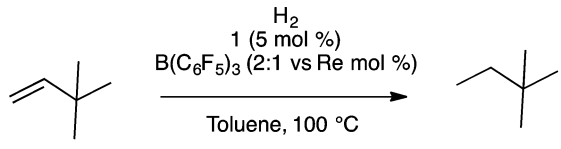

the order with respect to substrate, catalyst/cocatalyst, and hydrogen. The substrate chosen for the kinetic analysis was 3,3-dimethyl-1 butene (neohexene) because of the relative ease of ^{1}H NMR assignments. In addition, this substrate cannot undergo double-bond isomerization, thus simplifying the kinetic analysis.

The catalytic reaction exhibits first-order dependencies on **1**/$B(C_6F_5)_3$ and neohexene and a zeroth-order dependence on H_2 (Figure 4). Thus, the rate law for the overall catalytic reaction is given by eq 1:

$$\frac{d[\text{neohexane}]}{dt} = k[\text{neohexene}][\mathbf{1}/B(C_6F_5)_3] \quad (1)$$

In addition to these kinetic studies, the kinetic isotope effect (KIE) was determined when using D_2 instead of H_2 under previously optimized conditions. Time profiles for parallel reactions were monitored over time, and k_{obs}^{H} and k_{obs}^{D} values were extrapolated. From these experiments a KIE of 1.11(1) was obtained which suggests that H_2 activation does not occur in the turnover-limiting step.

Catalytic Competency of 2. Complex **2** was generated in situ and examined as a catalyst for the hydrogenation of neohexene (Scheme 4). When 1 equiv of $B(C_6F_5)_3$ was utilized in catalysis, the activity was approximately 10 times slower than the comparable reaction with an additional equiv of $B(C_6F_5)_3$ (Figure S8). The addition of up to 3.5 equiv does not result in any further increase in the rate of hydrogenation (see Figure S9 for complete dependence on $B(C_6F_5)_3$).

When **1** and 1 equiv of $B(C_6F_5)_3$ were utilized, the species identified at the end of the reaction was (DAP)Re(O)C_6F_5, **3**. In contrast, when 2 equiv of $B(C_6F_5)_3$ was used in the reaction, the species identified throughout the reaction was **2**. This establishes **2**, or the FLP generated from **2**, as the resting state of the catalytic system. The reduced rate observed with 1 equiv of $B(C_6F_5)_3$ results from competitive C_6F_5 transfer to **1** to produce **3**. As shown in Figure 5, catalysis with **3** is significantly slower than with **1**. The addition of excess equivalents of $B(C_6F_5)_3$ is necessary to prevent C_6F_5/Ph group exchange (Scheme 5).

Catalysis with Other Oxorhenium Catalysts. Other oxorhenium catalysts (Scheme 6, Figure 5) were explored in order to probe the steric and electronic demands of the reaction. Reduced rates were observed with catalysts **3** and **4**, bearing pentafluorophenyl and methyl substituents respectively, however, catalyst **5**, which contains the benzoyl substituent, exhibited similar reactivity to **1**. An induction period of ~250 min was

DOI: 10.1021/jacs.6b00705
J. Am. Chem. Soc. 2016, 138, 4832−4842

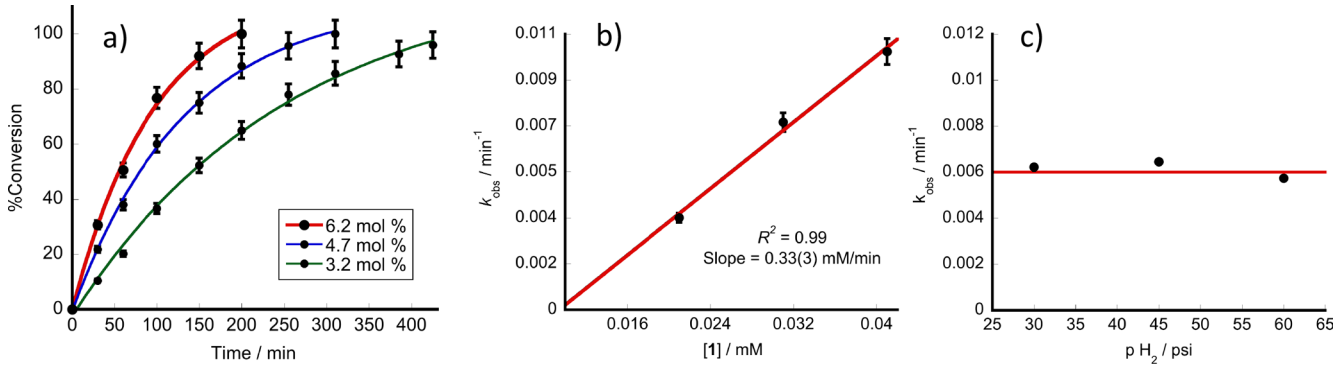

Figure 4. (a) Time profiles for hydrogenation of neohexene with **1**/$B(C_6F_5)_3$. Conditions: 2:1 B:Re: [**1**] = 0.021 mM, $[B(C_6F_5)_3]$ = 0.042 mM, (3.4 mol %); [**1**] = 0.031 mM, $[B(C_6F_5)_3]$ = 0.062 mM, (4.7 mol %); [**1**] = 0.041 mM, $[B(C_6F_5)_3]$ = 0.082 mM, (6.7 mol %); [olefin] = 0.62 mM. (b) Dependence of k_{obs} on [**1**]. (c) Dependence of k_{obs} on pH_2. Conditions: [**1**] = 0.020 mM; $[B(C_6F_5)_3]$ = 0.040 mM; [olefin] = 0.30 mM.

Scheme 4. Hydrogenation of Neohexene with 2 Generated in Situ

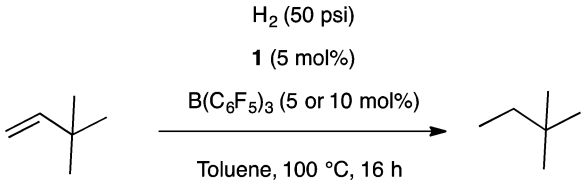

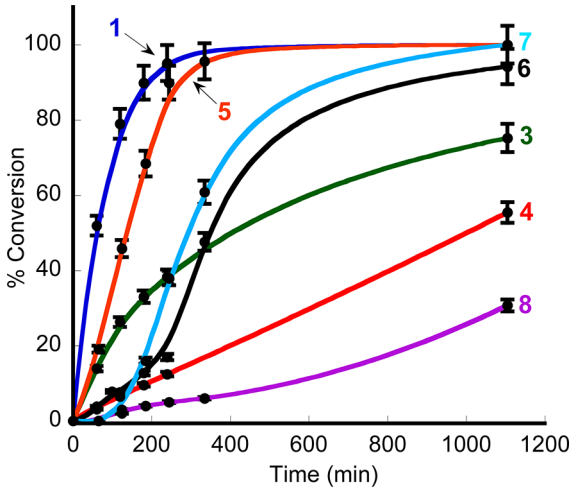

Figure 5. Competency of other oxorhenium catalysts. Conditions: [Re] = 0.0306 mM; $[B(C_6F_5)_3]$ = 0.0613 mM [olefin] = 0.613 mM. Conversions determined by ^{1}H NMR spectroscopy by integrating the ratios of *tert*-butyl singlets of the product with respect to the reactant.

Scheme 5. Competitive Formation of a FLP and 3 from 1 and $B(C_6F_5)_3$

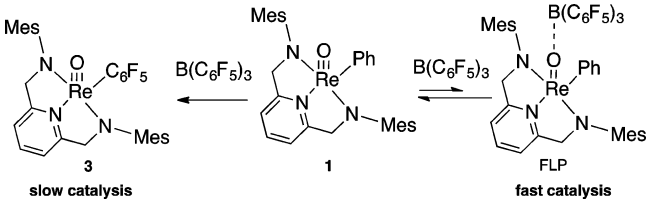

observed when the hydride complex **6** was used as a catalyst. Similarly an induction period (~200 min) was observed when methyltrioxorhenium (MTO) **7** was utilized.[14] Low conversions were obtained when the rhenium dioxo complex **8** was used as a catalyst, while complexes **9** and **10**, which contain a phenoxyoxazoline ligand, did not show any activity.[15]

Scheme 6. Olefin Hydrogenation with Oxorhenium Complexes

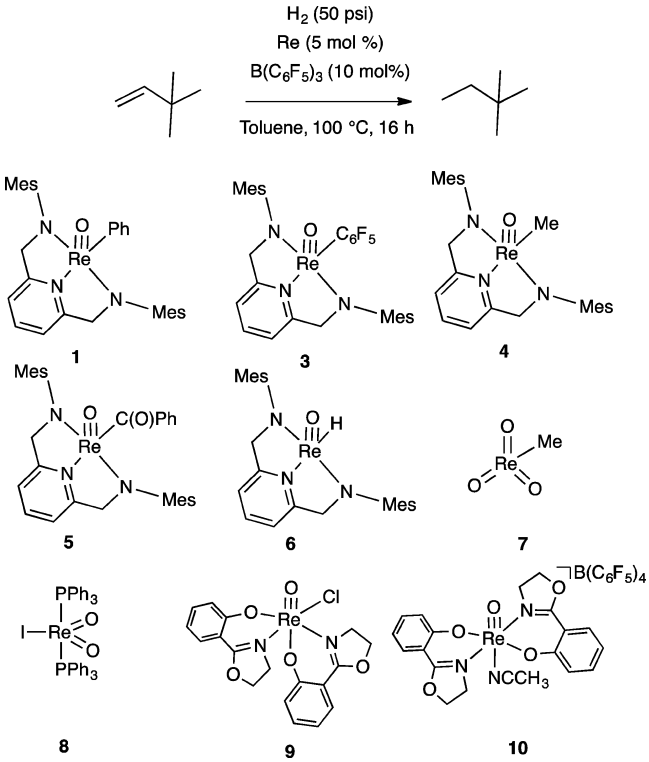

The Nature of the Induction Period for ***6****.* The most prominent induction period (~250 min) was observed with **6**. Notably, catalyst **4**, which contains a methyl substituent, proceeded at approximately the same rate compared to **6** during the induction period (Figure 5). We therefore sought to investigate the nature of the induction period and identify the possible catalytically active species along the reaction pathway.

Traditional Organometallic Mechanism. A Re−H could be potentially generated by a σ-bond metathesis of H_2 with **1**. Given that olefin insertion into Re−H bonds is a well-known reaction, we were prompted to explore the viability of an insertion/elimination pathway. One potential mechanism could involve the activation of the Re−H by coordination of $B(C_6F_5)_3$ to the oxo ligand in **6**. This would be followed by olefin insertion into the

DOI: 10.1021/jacs.6b00705
J. Am. Chem. Soc. 2016, 138, 4832−4842

Re−H bond and heterolytic cleavage of the rhenium alkyl bond with H_2 (Scheme 7).

Scheme 7. Traditional Organometallic Mechanism

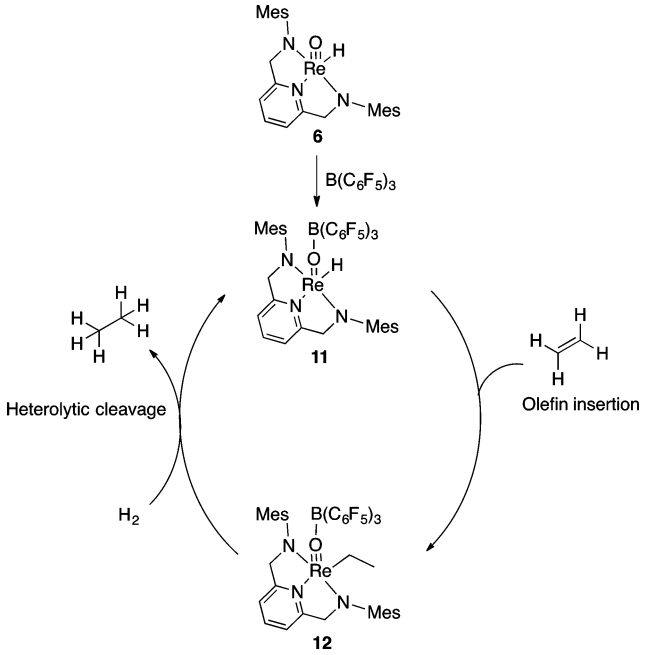

Similar to the formation of **2** (Scheme 1), treatment of complex **6** with $B(C_6F_5)_3$ in aromatic solvents yields the classical Lewis acid−base adduct **11**. X-ray quality crystals were obtained by vapor diffusion of pentane into the concentrated toluene solution of **11** (Figure 6). Similar to the structure for **2**, rhenium occupies a square pyramidal coordination environment in **11** with the oxo ligand in the apical position. The expected elongation of the Re−O bond is observed, due to the reduced bond order upon binding of Lewis acid. Other bond lengths are consistent with previously reported structures bearing the same ligand set.[3] The hydride ligand could not be located in the difference map, but other physical methods (described below) were used to confirm its presence.

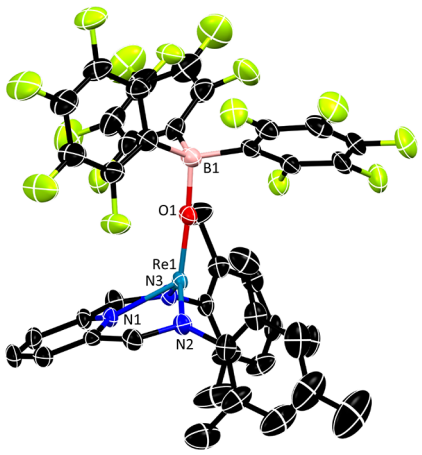

Figure 6. Thermal ellipsoid plot for **11**. Ellipsoids are at the 50% probability level. Hydrogen atoms were omitted for clarity. Selected bond lengths (Å) and angles (deg). Re1−O1, 1.757(3); Re1−N3, 1.939(4); Re1−N1, 2.042(4); Re1−N2, 1.947(4); O1−B1, 1.529(7) O1−Re1−N3, 113.51(18); O1−Re1−N2, 113.39(18); N3−Re1−N2, 133.09(19); O1−Re1−N1, 124.15(16); N3−Re1−N1, 76.63(16); N2−Re1−N1, 76.66(17); B1−O1−Re1, 175.3(4).

Complex **11** was characterized by ^{1}H, ^{13}C, ^{19}F, and NMR spectroscopy, X-ray crystallography, IR spectroscopy and elemental analysis. By ^{1}H NMR spectroscopy, the hydride resonance shifts from 6.02 ppm in **6** to 11.83 ppm in **11**. This signal is not observed in the deuterated analog **11-d** which was prepared in a similar fashion. The downfield shift for the hydride ligand in **11** is consistent with the increased acidity of the Re−H bond, because of the electron-withdrawing $B(C_6F_5)_3$. A shift of fluorine resonances to new frequencies is also observed in the ^{19}F NMR spectrum (Figure S2).

While the hydride precursor **6** does not show any reactivity with olefins, even at elevated temperatures, complex **11** smoothly reacts with a variety of olefins to yield the corresponding rhenium alkyl species. For example, the reaction of **11** with ethylene at 80 °C results in the formation of $(C_6F_5)_3B(O)Re(DAP)(Et)$, **12** (Scheme 8), which was characterized by ^{1}H, ^{13}C, and ^{19}F NMR spectroscopy (see Supporting Information). Complex **12** can also be synthesized from the reaction of (O)Re(DAP)(Et), **13**, with $B(C_6F_5)_3$.

Scheme 8. Synthesis of 12

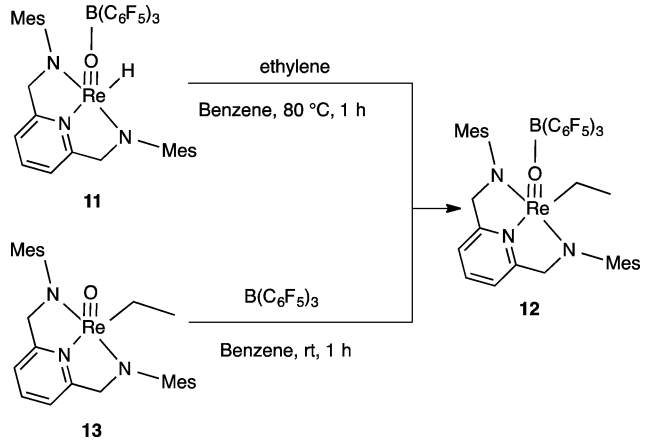

By ^{1}H NMR spectroscopy, **12** shows characteristic alkyl resonances corresponding to the ethyl ligand as well as a shift of diastereotopic methylene protons to different frequencies. Two additional signals belonging to the ethyl ligand are also observed by ^{13}C NMR spectroscopy.

When **12** was pressurized with H_2, no ethane was observed under optimized conditions (50 psi H_2, 100 °C). Complex **11** was also not observed. Instead, **12** displayed excellent stability even at higher temperatures. These results suggest that a traditional organometallic olefin insertion pathway as described in Scheme 7 is not a catalytically viable pathway for this reaction.

Identification of Catalytically Active Species. Two additional species were identified in catalytic reactions with **6**. Complex **3**, which contains the C_6F_5 group, was crystallized at the end of the catalytic reaction and characterized. This reactivity is not uncommon as pentafluorophenyl transfer can occur from borane Lewis acids to the metal center.[16] As shown above (Figure 5), **3** exhibits moderate activity for the hydrogenation of *t*-butylethylene (76% after 16 h).

Additionally, the cyclometalated product, **14**, was observed during the stoichiometric reaction of **6** with $B(C_6F_5)_3$ (Scheme 9). The cyclometalated product formed by C−H activation of mesityl substituent was observed by ^{1}H NMR spectroscopy, and

DOI: 10.1021/jacs.6b00705
J. Am. Chem. Soc. 2016, 138, 4832−4842

Scheme 9. Synthesis of 14

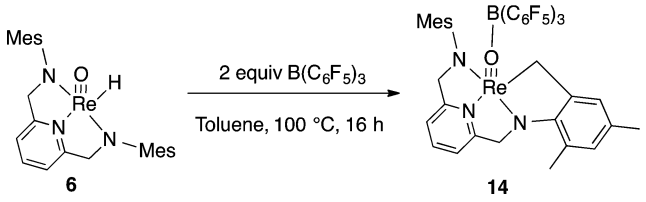

its structure was elucidated on the basis of chemical shifts and signal integrations (see Supporting Information). The ^{1}H NMR spectrum for **14** features five methyl signals for the mesityl ligands, as a result of the broken symmetry of the molecule, and C−H activation of the methyl fragment. Furthermore, six different diastereotopic methylene protons were observed in the expected region, indicating again different chemical environments due to the asymmetric nature of the compound. A similar cyclometalation reaction was observed by Schrock and coworkers for the C−H activation of a mesityl substituent of a Zr−Np complex bearing a diamidoamine ligand.[17] Complex **14** was found to be catalytically active in the hydrogenation of ethylene.

Reactions of **6** with $B(C_6F_5)_3$ under catalytic conditions are summarized in Scheme 10. Olefin insertion to produce **12** was

Scheme 10. Nature of Induction Period for 6

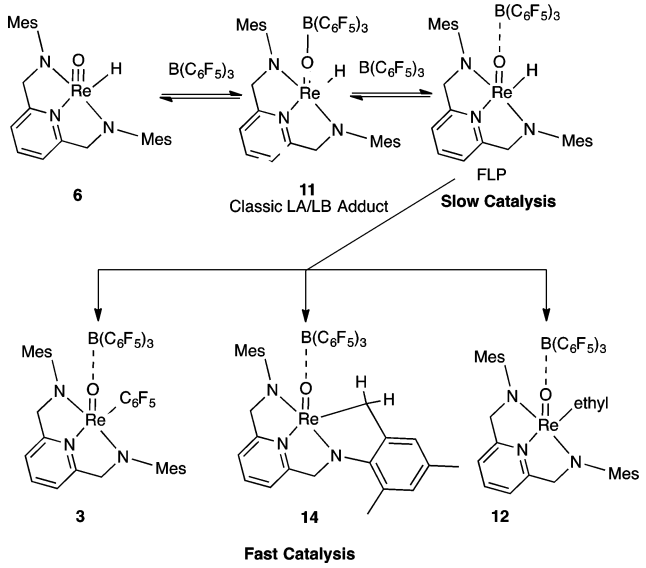

shown to be facile, however, cleavage of the rhenium carbon bond with H_2 does not occur, which suggests that this pathway is not a viable catalytic pathway. Complexes **3** and **14** are catalytically active (Figure S10), however, the major component of catalytic reactions is **12**. These data suggest that during catalysis with **6**, more active catalytic species (**3**, **12**, and **14**) are generated. This accounts for the sigmoidal behavior observed during catalysis. Olefin insertion into the Re−H bond also occurs, but since this pathway does not lead to catalysis, it is mainly a deactivation pathway.

Computational Studies. In order to gain additional insights into the reaction mechanism, DFT (B3PW91) calculations were performed. For these calculations, catalytic reactions employing catalyst **4** with ethylene were modeled because: (1) as shown in Figure 5, **4** shows significant albeit modest reactivity, (2) the size of the FLP generated from this complex and $B(C_6F_5)_3$ allows for accurate calculations at a reasonable computational time, and (3) as shown in Chart 1, ethylene was successfully hydrogenated under catalytic conditions. This last point is important because typical olefin hydrogenation mechanisms proceed by transient hydrogen activation by a FLP, followed by proton transfer to an olefin to form a carbocation, which subsequently leads to irreversible reaction with the hydridoborate to liberate the hydrocarbon and regenerate the FLP (Scheme 11).[1s,6b,18] Ethylene as a substrate allowed us to test the viability of this mechanism because protonation will result in the generation an unstable primary carbocation.

Structure optimizations included Grimme's D3 dispersion corrections[9] as implemented in Gaussian 09.[10] For these calculations Gibbs free energies at 373 K are reported and include solvation corrections by utilizing the PCM solvation model[11] with benzene as the solvent. The viability of a typical FLP mechanism for a system that involves oxorhenium complexes as the Lewis base component of the FLP was considered first.

Viability of Typical FLP Mechanism. As noted above, for the oxorhenium complexes examined, upon thermal activation, a FLP is generated that is capable of activating H_2 (Scheme 2). Thus, the FLP generated from **1** and $B(C_6F_5)_3$ was shown to scramble a mixture for H_2 and D_2.

H_2 splitting with **4**/$B(C_6F_5)_3$ was therefore investigated. The proposed FLP mechanism for the catalytic hydrogenation of ethylene is shown in Scheme 12. It begins with the generation of a FLP from the classical Lewis acid−base pair, **14**. This FLP activates H_2 to generate the onium hydridoborate, **16**, which activates ethylene by sequential protonation to form a cation, followed by hydride transfer from the hydridoborate portion of **17**. Each of the steps is analyzed in detail below.

FLP Generation: The Structure and Bonding in FLPs. The optimized structures of frustrated Lewis acid pairs generated from **1**, **4**, and **6** are depicted in Figure 7. Interaction of $B(C_6F_5)_3$ with the rhenium oxo bond generates the frustrated Lewis acid pairs, **18**, **15**, and **19**, respectively. For **15** the formation of this FLP from the infinitely separated $B(C_6F_5)_3$ and (O)Re(DAP)-(Me) fragment is slightly endergonic (ΔG_{373} = 1.09 kcal/mol) and is generated from the classical Lewis acid−base pair **14**, (ΔG_{373} = −16.8 kcal/mol) which proceeds through the transition state (TS)**TS(14−15)** ($\Delta G^{\ddagger}$ = 6.30 kcal/mol).

The most important characteristic of FLPs **18**, **15**, and **19** is the long B−O bond lengths (3.67 Å, **18**; 3.74 Å, **15**; 3.65 Å, **19**).

Scheme 11. Typical Mechanism for Olefin Hydrogenation with FLPs

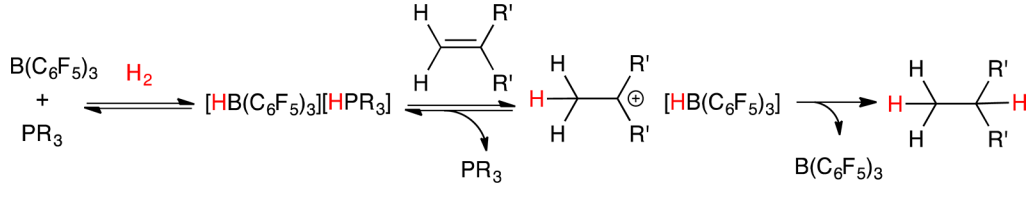

DOI: 10.1021/jacs.6b00705
J. Am. Chem. Soc. 2016, 138, 4832−4842

Scheme 12. Proposed FLP Mechanism with Oxorhenium Catalysts

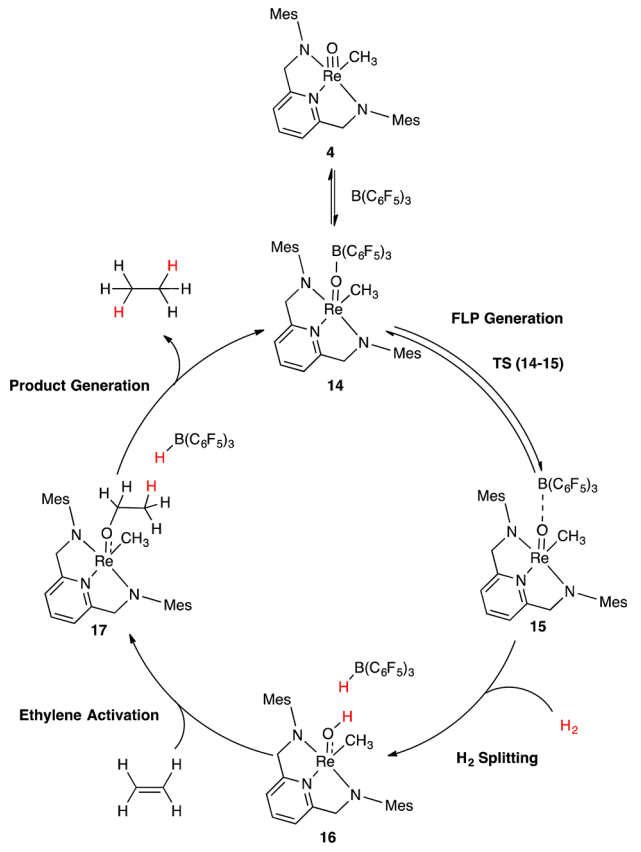

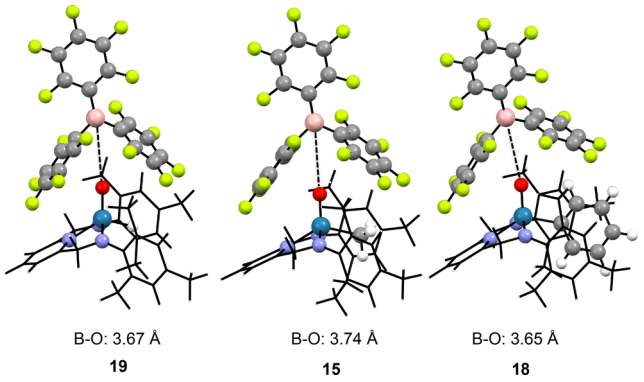

Figure 7. B3PW91+D3 calculated structure for FLPs **19** (Re−Ph), **15** (Re−Me), and **18** (Re−H).

Further, the plane formed by B and the three C_6F_5 rings is now parallel to the Re═O bond, suggesting that there is an absence of a dative bond between the oxo and $B(C_6F_5)_3$. This is illustrated further in the lowest unoccupied molecular orbital (LUMO) for **15**, where it is shown that the electron density is localized on the $B(C_6F_5)_3$ fragment (see Figure 10).

The structural characteristics and the nature of the B−O bond length are quite similar to the traditional organic FLPs. For example Zeonjuk and co-workers have calculated the optimal distances necessary for FLP reactivity between the boron and phosphorus atoms. This range was estimated to be from 3 to 5 Å between the boron and phosphorus metal center. For example, the calculated equilibrium structure of the well-understood $Mes_3P-B(C_6F_5)_3$ FLP has a calculated B−P bond distance of 3.86 Å.[19] This correlates well with the calculated distance for the highest active catalyst generated from **1**.

A more in depth analysis of the bonding in the calculated FLP structures reveals several interesting features (Figure S28). Two of the aryl rings are oriented perpendicular to the Re−oxo bond in **15**. The distances of the oxo ligand to the center of these rings are 2.68 and 3.39 Å at angles of 125° and 126°, respectively. These values are reminiscent of the studies of main group FLPs (t-Bu_3P:$B(C_6F_5)_3$) by Rhee and co-workers.[20] Further, within this structure there is one H−F bond between the Mes methyl groups on the diamidopyridine ligand and the C_6F_5 groups on $B(C_6F_5)_3$ at a distance of 2.49 Å and an angle of 112°. Given that the idealized bond lengths and angles for H−F hydrogen bonding are <2.5 Å and 180°, these data suggest that hydrogen bonding may not be a significant factor in stabilizing FLPs and that the stability may be driven by similar lone-pair (Re═O) to π orbital (from the C_6F_5 group of $B(C_6F_5)_3$) interactions as observed by Rhee.[1r] However, unlike main group FLPs, a direct P−B interaction as in classical Lewis pairs does not appear to exist. This is evident in Figure 7 as the plane encompassing the boron atom and its aryl substituent is oriented orthogonal to the lone pair on the Re═O.

H_2 Splitting. At 373 K splitting of H_2 by **15** is endergonic (ΔG_{373} = 8.47 kcal/mol) (Scheme 13). However, it was observed

Scheme 13. Splitting of H_2 by 15[a]

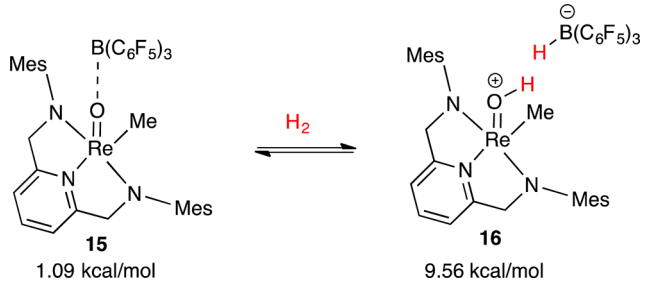

[a]Free energies (373 K) are reported relative to the infinitely separated species **4**, H_2, and ethylene.

experimentally that FLPs generated from oxorhenium complexes resulted in the scrambling of H_2/D_2 mixtures (Scheme 2). This suggests that the barrier for H_2 splitting by these complexes is low. The data are also consistent with previously reported reactivity of main group FLPs that have been shown to lead to facile H_2 splitting at mild temperatures.[1m,q] Thus, the activation of ethylene with **16** was explored with this catalytic system.

Ethylene Activation. Typically, olefin activation by main group FLPs is believed to proceed by initial protonation to generate a carbocation, followed by irreversible hydride transfer from a hydridoborate.[1s,6b] Electron-rich olefins are typically employed to stabilize the carbocation intermediate that results from protonation. In the case of ethylene, a primary carbocation would be generated, as a result catalytic hydrogenation with main group FLPs is generally not effective with unactivated olefins. In order to test the viability of the typical FLP mechanism in the catalytic system described here, we examined ethylene activation with **16**.

The activation of ethylene by **16** proceeds with unreasonably high barriers to generate a new classical borane $(C_6F_5)_2$((6-Et-1-H-C_6F_5)B·(O)Re(DAP)(Me), **22** (Figure S30), ($\Delta G^{\ddagger}_{373}$ = 45.3 kcal/mol) or to oxidize ethylene to ethanol with the subsequent reduction of the Re(V) component to Re(III) (Figure S31),

DOI: 10.1021/jacs.6b00705
J. Am. Chem. Soc. 2016, 138, 4832−4842

($\Delta G^{\ddagger}_{373}$ = 73.7 kcal/mol). Importantly, neither of the reactions depicted in Figures S30 and S31 result in the formation of ethane. Thus, the data suggest that the activation of ethylene via initial proton transfer to generate a carbocation is unlikely for this catalytic system. In fact, results suggest that the carbocation generated is so reactive that it reacts either with the electron-rich aryl ring to generate **21** or abstracts the oxo ligand to generate **23**.

Hydride Transfer. The viability of hydride transfer from the hydridoborate portion of **16** was also investigated. As shown in Figure 8, the formation of the alkoxy complex **24** from **16** is

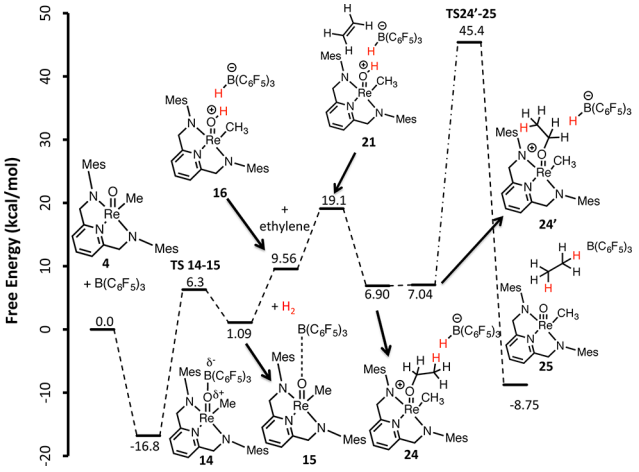

Figure 8. Free energy (373 K) for hydride transfer from the hydridoborate portion of **16**.

exergonic at 373 K (ΔG_{373} = −2.66 kcal/mol). However, hydride transfer occurs with an activation barrier ($\Delta G^{\ddagger}$) of 45.4 kcal/mol. Thus, the data suggest that hydride transfer is also inaccessible at the reaction temperature employed.

To summarize, FLPs generated from the oxorhenium complexes effectively split H_2. However, the onium hydridoborate generated is not kinetically competent to activate ethylene via protonation or transfer a hydride to an oxo alkyl from the hydridoborate. Thus, these results suggest that a typical FLP mechanism is not viable for this catalytic system.

Concerted Attack of Frustrated Lewis Acid−Base Pairs on Olefinic Double Bonds. Having shown that a mechanism that involves initial H_2 splitting followed by sequential protonation and hydride transfer is not viable in this catalytic system, alternative mechanisms were explored. Stephan and co-workers have shown that ethylene and other alkenes react readily with mixtures of P(*t*-Bu)$_3$ and B(C_6F_5)$_3$ to yield products where the phosphine and borane add across the olefinic double bond.[21] In addition, Erker and co-workers have developed the intramolecular version of this reaction with P/B FLPs.[22] Further, theoretical studies by Papai and co-workers have shown that the Lewis acid and base centers act in concert in a FLP and lead to activation of the π-bond of the olefin and regio and stereoselective B−C and P−C covalent-bond formation.[23]

Despite the apparent facile reactivity of FLPs with olefins, to the best of our knowledge, a hydrogenation mechanism involving initial concerted olefin addition has not been considered. As a result we investigated a new mechanism that begins with initial activation of the olefin, followed by fast H_2 activation. Importantly, such a mechanism is consistent with the experimental kinetic data, where a first-order dependence on olefin and a zeroth-order dependence on H_2 were observed (see Figure 4).

The calculated mechanism for the catalytic hydrogenation of ethylene with **4** is depicted in Figure 9. This catalytic cycle begins

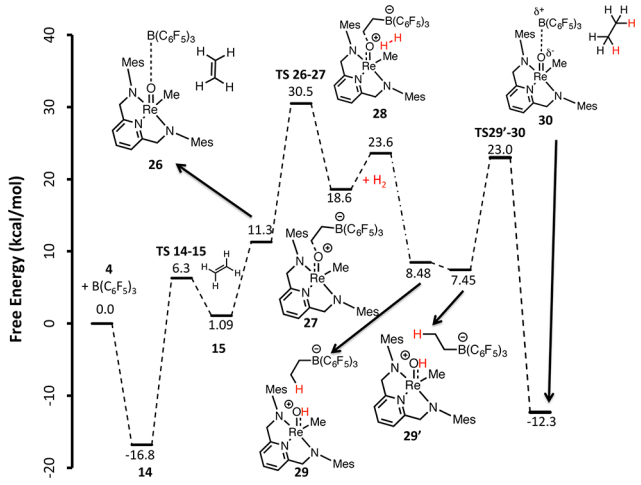

Figure 9. Free energy (373 K) for the concerted attack of the frustrated Lewis acid−base pair, **15**, on the olefinic double bond of ethylene.

with the formation of the FLP **15** from the classical Lewis acid−base adduct **14**. This is followed by olefin activation via the association complex, **26**, to generate zwitterion, **27**. Hydrogen cleavage occurs by addition across the polarized Re=O → CH_2CH_2(B(C_6F_5)$_3$) bond in **27** to generate the ion pair, [((Et)B(C_6F_5)$_3$)][H(O)Re(DAP)(Me)], **29**, which subsequently rearranges to its isomer **29′**. The acidic Re=OH group in **29** results in protonation of the ethyl fragment in the Et(B(C_6F_5)$_3$) group to release of ethane and regenerate the catalytic cycle. Importantly, the highest barrier (30.5 kcal/mol) for this mechanism is the olefin activation step, which is consistent with the kinetic data presented above.

Analysis of the key species for the critical steps of the calculated mechanism (olefin activation, hydrogen cleavage, proton transfer) is described below.

Olefin Activation. The LUMO depicted in Figure 10 suggests that the B(C_6F_5)$_3$ in **15** is perfectly aligned for electrophilic activation of the olefin. Addition of the (O)Re(DAP)(Me) and B(C_6F_5)$_3$ fragments across the olefin is endergonic (ΔG_{373} = 7.3 kcal/mol) and results in the formation of the zwitterion, **27** via

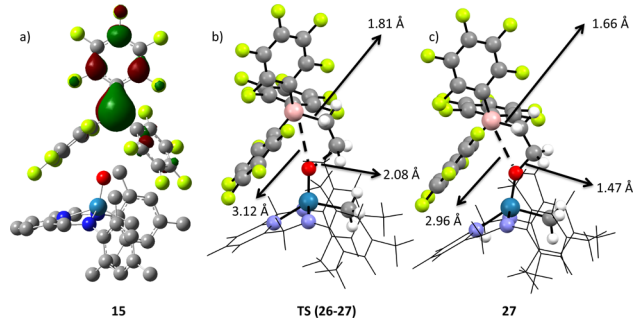

Figure 10. (a) B3PW91+D3 calculated LUMO for FLP generated from **4**. Kohn−Sham orbitals are depicted using an isocontour value of 0.045. (b) Optimized structure for **TS(26−27)** with selected bond lengths. (c) Optimized structure for **27** with selected bond lengths.

DOI: 10.1021/jacs.6b00705
J. Am. Chem. Soc. 2016, 138, 4832−4842

TS(26−27) ($\Delta G^{\ddagger}$ = 19.2 kcal/mol). The optimized structures for **26** and **TS (26−27)** are depicted in Figure 10.

Multiple bond character in the rhenium oxo bond[20,24] is maintained in both **TS (26−27)** and in **27** as both species exhibit short bonds to the oxo ligand (1.72 and 1.77 Å, respectively). The transition state for the addition of ethylene involves an asynchronous concerted cis 1,2-addition of the olefin to the boron and oxygen atoms in **26** with boron−carbon bond formation preceding oxygen−carbon bond formation. This is evident by inspection of the B−C and C−O Wiberg bond orders[25] (0.617 and 0.236, respectively) and bond lengths (1.81 and 2.08 Å respectively). The *cis*-olefin addition observed here is in contrast to the *trans*-olefin addition observed by Li,[26] Stephan,[21] and Papai.[27] However, the data are consistent with the *cis*-olefin addition observed by Erker and co-workers.[22c] In fact the B−C bond length observed in **TS (26−27)** (1.81 Å) is similar to the TS reported by the Erker group (1.83 Å) for the addition of an intramolecular FLP to norbornene.[22c]

Hydrogen Cleavage. As shown in Scheme 14, three pathways were explored for the addition of H_2 to **27**. In the first pathway,

Scheme 14. Pathway for the Addition of H_2 to 27[a]

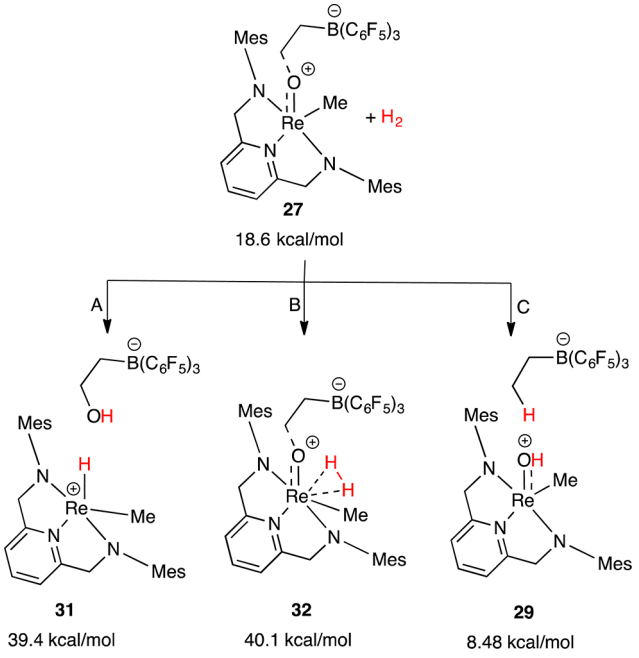

[a]Free energies (373 K) are reported relative to the infinitely separated species **4**, H_2, and ethylene.

addition of hydrogen across the rhenium oxo bond (σ bond metathesis) leads to [HRe(DAP)(Me][$HOCH_2CH_2B(C_6F_5)_3$], **31**. Pathway B involves the activation of H_2 at Re via the dihydrogen adduct, **32**, and last, pathway C involves cleavage of the oxygen−carbon bond in **27** to produce **29**. At 373 K, pathways A and B are endergonic with free energies of 20.8 and 21.5 kcal/mol, respectively. In contrast, hydrogenolysis of the carbon−oxygen bond in **27** is exergonic (ΔG_{373} = −10.1 kcal/mol). The unstable nature of **31** and **32** suggests that hydrogen cleavage does not proceed through these species. Further, given that these intermediates are higher in energy than **TS (26−27)**, hydrogen cleavage through these intermediates is unlikely since the kinetics for the catalytic reaction suggest that olefin activation is the turnover-limiting step. Structure **27** maintains Re−oxo multiple bond character (1.77 Å). For example, by comparison, the Re−OEt bond in *trans*-$ReOCl_2(OEt)(t\text{-}Bu_2P(OEt)(t\text{-}Bu_2P(H)O)$[28] is significantly longer (1.85(2) Å). Further, the carbon−oxygen bond length is significantly longer in **27** (1.47 Å) than in *trans*-$ReOCl_2(OEt)(t\text{-}Bu_2P(OEt)(t\text{-}Bu_2P(H)O)$ (1.41 Å). These factors result in the facile cleavage of the C−O bond in **27** by H_2.

Product Generation. Product is generated from **29′** via proton transfer from the acidic Re═OH group to the alkyl fragment in $EtB(C_6F_5)_3$. This step proceeds via **TS(29′-30)**, with an activation barrier of 23.0 kcal/mol. The acidity of hydroxyl groups on rhenium has been noted by Neurock and co-workers, as these groups have been proposed to be responsible for the hydrogenolysis of polyols and cyclic ethers.[29] This acidity of the hydroxyl groups is derived from the electron affinity of the high-valent oxo, which depletes electron density from the OH bond and ultimately results in the generation of a proton. In contrast, as noted above, (see Figure 8) transfer of a hydride to a rhenium alkoxy ligand proceeds with a significantly higher barrier (45.4 kcal/mol). Thus, unlike hydride transfer to a rhenium alkoxy ligand which was shown not to be kinetically competent, proton transfer from an acidic hydroxyl group is facile under reaction conditions.

To summarize, the mechanism most consistent with the computational and experimental data is depicted in Scheme 15.

Scheme 15. Summary of the Proposed Mechanism for the Catalytic Hydrogenation of Olefins with FLPs Generated from Transition-Metal Oxos

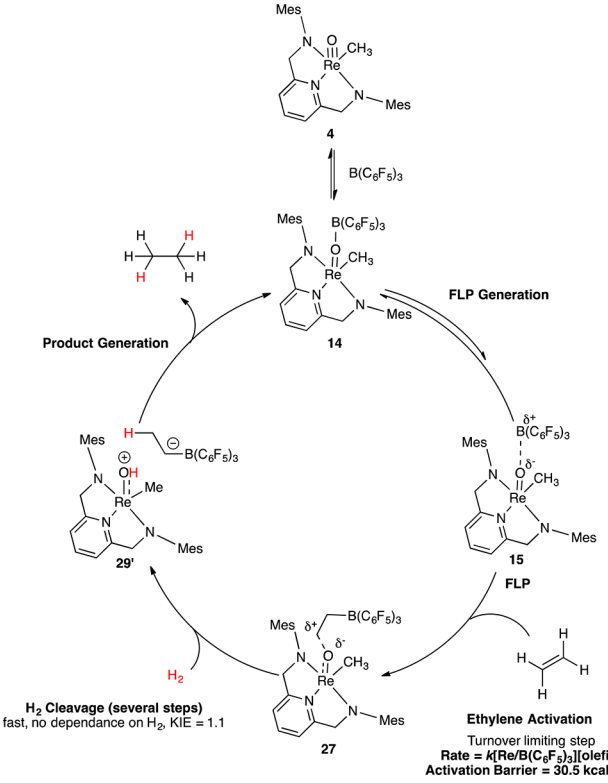

The addition of $B(C_6F_5)_3$ to **4** results in the generation of a FLP, **15**. Concerted attack of this FLP across the double bond of ethylene is the turnover-limiting step. Fast H_2 cleavage then occurs to generate an acidic hydroxyl group that protonates an alkyl borate to generate the product. This mechanism is consistent with the empirical rate law and is also consistent with the observed insignificant H/D kinetic isotope effect.

DOI: 10.1021/jacs.6b00705
J. Am. Chem. Soc. 2016, 138, 4832−4842

CONCLUSIONS

Oxorhenium/borane adducts have been shown to be catalytically competent for the hydrogenation of unactivated olefins. Good conversions of olefins to alkanes were obtained for a variety of terminal, internal, and cyclic olefins. Kinetic studies indicate first-order rate dependencies on [rhenium/cocatalyst] and [substrate] and a zero-order dependence on molecular hydrogen. In addition a KIE of 1.11(1) was obtained from parallel reactions with H_2 and D_2 These data suggest that H_2 activation does not occur in the turnover-limiting step. Mechanistic studies indicate that the oxorhenium complexes interact with $B(C_6F_5)_3$ to form a FLP. This results in electrophilic activation of the olefin and ultimately heterolytic cleavage with H_2. The mechanism presented fundamentally differs from traditional transition-metal-catalyzed hydrogenation in that catalysis does not involve coordination of the substrates to the metal center.[30] Other rhenium catalysts were shown to exhibit catalytic activity. Preliminary evidence suggests that catalytic activity correlates with the sterics of the X-type ligand bound to rhenium.

EXPERIMENTAL SECTION

General Considerations. Complexes **1**, **4**, **5**, **6**, **9**,[15] and **10**[15] were prepared as previously reported;[31] all other reagents were purchased from commercial resources and used as received. $B(C_6F_5)_3$ was purchased from Strem Chemicals and sublimed prior to use. ^1H, ^{13}C, ^{19}F NMR spectra were obtained on 300 or 400 MHz spectrometers at room temperature. Chemical shifts are listed in parts per million (ppm) and referenced to their residual protons or carbons of the deuterated solvents, respectively. All reactions were run under an inert atmosphere with dry solvents unless otherwise noted. High-pressure reactions were performed in a stainless steel Micro Bench Top Reactor. FTIR spectra were obtained in KBr thin films. Elemental analyses were performed by Atlantic Micro Laboratories, Inc.

Computational Methods. Computations were performed on clusters provided by NC State Office of Information Technology High Performance Computing (HPC). Theoretical calculations have been carried out using the Gaussian 09[10] implementation of B3PW91[4] density functional theory. All geometry optimizations were carried out in the gas phase using tight convergence criteria ("opt = tight") and pruned ultrafine grids ("Int = ultrafine"). The basis set for rhenium was the small-core (311111,22111,411) → [6s5p3d] Stuttgart–Dresden basis set and relativistic effective core potential combination (SDD)[8] with an additional *f* polarization function.[7b] The 6-31G(d,p)[7a] basis set was used for all other atoms. Cartesian *d* functions were used throughout, i.e., there are six angular basis functions per *d* function. Calculations also include dispersion effects by utilizing Grimme's D3 dispersion correction with Becke–Johnson damping.[9] All structures were fully optimized, and analytical frequency calculations were performed on all structures to ensure either a zeroth-order saddle point (a local minimum) or a first-order saddle point (TS) was achieved. The minima associated with each transition state was determined by animation of the imaginary frequency and, if necessary, with intrinsic reaction coordinate (IRC) calculations.

Energetics were calculated at 373 K with the 6-311++G(d,p)[32] basis set for C, H, N, O, and F atoms and the SDD basis set with an added *f* polarization function on Re. Reported energies utilized analytical frequencies and the zero-point corrections from the gas phase optimized geometries and included solvation corrections which were computed using the PCM method, with benzene as the solvent as implemented in Gaussian 09.

ASSOCIATED CONTENT

Supporting Information

The Supporting Information is available free of charge on the ACS Publications website at DOI: 10.1021/jacs.6b00705.

Kinetic data. Experimental details for the synthesis of **2**, **3**, **11**, and **14**. Computational details. Full Gaussian reference. Computational coordinates and XYZ files (PDF)

Crystallographic data for **2**, **3**, and **11** (CIF)

Computational data (XYZ)

AUTHOR INFORMATION

Corresponding Author

*eaison@ncsu.edu

Notes

The authors declare no competing financial interest.

ACKNOWLEDGMENTS

We acknowledge North Carolina State University and the National Science Foundation via the CAREER Award (CHE-0955636) for funding.

REFERENCES

(1) (a) Stephan, D. W. *J. Am. Chem. Soc.* **2015**, *137*, 10018–10032. (b) Stephan, D. W.; Erker, G. *Angew. Chem., Int. Ed.* **2015**, *54*, 6400–6441. (c) Paradies, J. *Angew. Chem., Int. Ed.* **2014**, *53*, 3552–3557. (d) Houghton, A. Y.; Hurmalainen, J.; Mansikkamaki, A.; Piers, W. E.; Tuononen, H. M. *Nat. Chem.* **2014**, *6*, 983–988. (e) Stephan, D. W.; Erker, G. *Chem. Sci.* **2014**, *5*, 2625–2641. (f) Mahdi, T.; Stephan, D. W. *Angew. Chem., Int. Ed.* **2013**, *52*, 12418–12421. (g) Berke, H.; Jiang, Y. F.; Yang, X. H.; Jiang, C. F.; Chakraborty, S.; Landwehr, A. *Top. Curr. Chem.* **2013**, *334*, 27–57. (h) Lu, Z. P.; Ye, H. Y.; Wang, H. D. *Top. Curr. Chem.* **2012**, *334*, 59–80. (i) Stephan, D. W.; Erker, G. *Top. Curr. Chem.* **2013**, *332*, 85–110. (j) Chernichenko, K.; Madarasz, A.; Papai, I.; Nieger, M.; Leskela, M.; Repo, T. *Nat. Chem.* **2013**, *5*, 718–723. (k) Stephan, D. W. *Org. Biomol. Chem.* **2012**, *10*, 5740–5746. (l) Ghattas, G.; Chen, D. J.; Pan, F. F.; Klankermayer, J. *Dalton Trans.* **2012**, *41*, 9026–9028. (m) Stephan, D. W. *Org. Biomol. Chem.* **2012**, *10*, 5740–5746. (n) Soos, T. *Pure Appl. Chem.* **2011**, *83*, 667–675. (o) Berkefeld, A.; Piers, W. E.; Parvez, M. *J. Am. Chem. Soc.* **2010**, *132*, 10660–10661. (p) Eros, G.; Mehdi, H.; Papai, I.; Rokob, T. A.; Kiraly, P.; Tarkanyi, G.; Soos, T. *Angew. Chem., Int. Ed.* **2010**, *49*, 6559–6563. (q) Geier, S. J.; Stephan, D. W. *J. Am. Chem. Soc.* **2009**, *131*, 3476. (r) Kim, H. W.; Rhee, Y. M. *Chem. - Eur. J.* **2009**, *15*, 13348–13355. (s) Chase, P. A.; Stephan, D. W. *Angew. Chem., Int. Ed.* **2008**, *47*, 7433–7437.

(2) (a) Metters, O. J.; Forrest, S. J. K.; Sparkes, H. A.; Manners, I.; Wass, D. F. *J. Am. Chem. Soc.* **2016**, *138*, 1994–2003. (b) Flynn, S. R.; Metters, O. J.; Manners, I.; Wass, D. F. *Organometallics* **2016**, *35*, 847. (c) Cui, P.; Comanescu, C. C.; Iluc, V. M. *Chem. Commun.* **2015**, *51*, 6206–6209. (d) Xu, X.; Kehr, G.; Daniliuc, C. G.; Erker, G. *J. Am. Chem. Soc.* **2015**, *137*, 4550–4557. (e) Dobrovetsky, R.; Stephan, D. W. *Isr. J. Chem.* **2015**, *55*, 206–209. (f) Boone, M. P.; Stephan, D. W. *Organometallics* **2014**, *33*, 387–393. (g) Fromel, S.; Kehr, G.; Frohlich, R.; Daniliuc, C. G.; Erker, G. *Dalton Trans.* **2013**, *42*, 14531–14536. (h) DeMott, J. C.; Bhuvanesh, N.; Ozerov, O. V. *Chem. Sci.* **2013**, *4*, 642–649. (i) Xu, X.; Kehr, G.; Daniliuc, C. G.; Erker, G. *Organometallics* **2013**, *32*, 7306–7311. (j) Xu, X.; Kehr, G.; Daniliuc, C. G.; Erker, G. *Angew. Chem., Int. Ed.* **2013**, *52*, 13629–13632. (k) Flynn, S. R.; Wass, D. F. *ACS Catal.* **2013**, *3*, 2574–2581. (l) Erker, G. *Dalton Trans.* **2011**, *40*, 7475–7483. (m) Miller, A. J. M.; Labinger, J. A.; Bercaw, J. E. *J. Am. Chem. Soc.* **2010**, *132*, 3301.

(3) Smeltz, J. L.; Lilly, C. P.; Boyle, P. D.; Ison, E. A. *J. Am. Chem. Soc.* **2013**, *135*, 9433–9441.

(4) Burke, K.; Perdew, J. P.; Wang, Y. Derivation of a generalized gradient approximation: The PW91 density functional. In *Electronic Density Functional Theory*; Springer: New York, 1998; pp 81–111.

(5) (a) Lindqvist, M.; Sarnela, N.; Sumerin, V.; Chernichenko, K.; Leskela, M.; Repo, T. *Dalton Trans.* **2012**, *41*, 4310–4312. (b) Rokob,

DOI: 10.1021/jacs.6b00705
J. Am. Chem. Soc. 2016, 138, 4832–4842

T. A.; Hamza, A.; Stirling, A.; Papai, I. *J. Am. Chem. Soc.* **2009**, *131*, 2029−2036.
(6) (a) Nicasio, J. A.; Steinberg, S.; Ines, B.; Alcarazo, M. *Chem. - Eur. J.* **2013**, *19*, 11016−11020. (b) Paradies, J. *Synlett* **2013**, *24*, 777−780.
(7) (a) Hariharan, P. C.; Pople, J. A. *Theoret. Chim. Acta* **1973**, *28*, 213−222. (b) Hehre, W. J.; Ditchfield, R.; Pople, J. A. *J. Chem. Phys.* **1972**, *56*, 2257−2261.
(8) Andrae, D.; Haeussermann, U.; Dolg, M.; Stoll, H.; Preuss, H. *Theoret. Chim. Acta* **1990**, *77*, 123−141.
(9) (a) Grimme, S.; Antony, J.; Ehrlich, S.; Krieg, H. *J. Chem. Phys.* **2010**, *132*, 154104. (b) Grimme, S.; Ehrlich, S.; Goerigk, L. *J. Comput. Chem.* **2011**, *32*, 1456−1465.
(10) Frisch, M. J.; Trucks, G. W.; Schlegel, H. B.; Scuseria, G. E.; Robb, M. A.; Cheeseman, J. R.; Scalmani, G.; Barone, V.; Mennucci, B.; Petersson, G. A.; et al. *Gaussian 09*; Gaussian Inc.: Wallingford, CT, 2009.
(11) Tomasi, J.; Mennucci, B.; Cances, E. *J. Mol. Struct.: THEOCHEM* **1999**, *464*, 211−226.
(12) Sandstrom, J. *Dynamic NMR Spectroscopy*; Academic Press Inc. Ltd.: London, 1982.
(13) While most of the starting olefin was converted in this case, the reaction produced a mixture of hexane (33%) and two isomers of hexene 2-hexene and 3-hexene (66%). This was presumably because there was insufficient H_2 to completely hydrogenate this substrate.
(14) The induction period observed for MTO is not understood at this time.
(15) (a) Ison, E. A.; Corbin, R. A.; Abu-Omar, M. M. *J. Am. Chem. Soc.* **2005**, *127*, 11938−11939. (b) Ison, E. A.; Trivedi, E. R.; Corbin, R. A.; Abu-Omar, M. M. *J. Am. Chem. Soc.* **2005**, *127*, 15374−15375.
(16) Kalamarides, H. A.; Iyer, S.; Lipian, J.; Rhodes, L. F.; Day, C. *Organometallics* **2000**, *19*, 3983−3990.
(17) Schrodi, Y.; Schrock, R. R.; Bonitatebus, P. J. *Organometallics* **2001**, *20*, 3560−3573.
(18) Hounjet, L. J.; Bannwarth, C.; Garon, C. N.; Caputo, C. B.; Grimme, S.; Stephan, D. W. *Angew. Chem., Int. Ed.* **2013**, *52*, 7492−7495.
(19) Zeonjuk, L. L.; Vankova, N.; Mavrandonakis, A.; Heine, T.; Röschenthaler, G.-V.; Eicher, J. *Chem. - Eur. J.* **2013**, *19*, 17413−17424.
(20) Herrmann, W. A.; Roesky, P. W.; Wang, M.; Scherer, W. *Organometallics* **1994**, *13*, 4531−4535.
(21) McCahill, J. S. J.; Welch, G. C.; Stephan, D. W. *Angew. Chem., Int. Ed.* **2007**, *46*, 4968−4971.
(22) (a) Voss, T.; Sortais, J.-B.; Fröhlich, R.; Kehr, G.; Erker, G. *Organometallics* **2011**, *30*, 584−594. (b) Sortais, J. B.; Voss, T.; Kehr, G.; Frohlich, R.; Erker, G. *Chem. Commun.* **2009**, 7417−7418. (c) Momming, C. M.; Fromel, S.; Kehr, G.; Frohlich, R.; Grimme, S.; Erker, G. *J. Am. Chem. Soc.* **2009**, *131*, 12280−12289.
(23) Bako, I.; Stirling, A.; Balint, S.; Papai, I. *Dalton Trans.* **2012**, *41*, 9023−9025.
(24) Mayer, J. M. *Inorg. Chem.* **1988**, *27*, 3899−3903.
(25) Glendening, E. D.; Weinhold, F. *J. Comput. Chem.* **1998**, *19*, 610−627.
(26) Guo, Y.; Li, S. *Eur. J. Inorg. Chem.* **2008**, *2008*, 2501−2505.
(27) Stirling, A.; Hamza, A.; Rokob, T. A.; Papai, I. *Chem. Commun.* **2008**, 3148−3150.
(28) Arif, A. M.; Bright, T. A.; Jones, R. A. *J. Coord. Chem.* **1987**, *16*, 45−50.
(29) Chia, M.; Pagán-Torres, Y. J.; Hibbitts, D.; Tan, Q.; Pham, H. N.; Datye, A. K.; Neurock, M.; Davis, R. J.; Dumesic, J. A. *J. Am. Chem. Soc.* **2011**, *133*, 12675−12689.
(30) Boone, M. P.; Stephan, D. W. *J. Am. Chem. Soc.* **2013**, *135*, 8508−8511.
(31) (a) Lilly, C. P.; Boyle, P. D.; Ison, E. A. *Dalton Trans.* **2011**, *40*, 11815−11821. (b) Lilly, C. P.; Boyle, P. D.; Ison, E. A. *Organometallics* **2012**, *31*, 4295−4301.
(32) Clark, T.; Chandrasekhar, J.; Spitznagel, G. W.; Schleyer, P. V. R. *J. Comput. Chem.* **1983**, *4*, 294−301.

DOI: 10.1021/jacs.6b00705
J. Am. Chem. Soc. 2016, 138, 4832−4842